Feasibility Study of a Mission to Remove Eight SL-8 Rocket Boosters from LEO

KTH Royal Institute of Technology
MSc in Aerospace Engineering
October 19^{th}, 2022

MScAE Francesc Hernández Garcia, Marcus Mhanna, Ngai Nam Chan, and Simon Lilja

***Abstract*—This paper presents a conceptual feasibility study of an active debris removal mission aiming to deorbit eight SL-8 Rocket Boosters from Low Earth Orbit (LEO). This is done by designing a satellite system consisting of eight CubeSat-based spacecraft, which will be deployed from a parking orbit. Each spacecraft will employ low thrust propulsion to approach a SL-8 booster, which will be captured and deorbited using a tethered net. The main subsystems of each spacecraft are conceptually designed. This includes power, structure, propulsion, communications and Attitude Determination and Control System (ADCS). The mission features in terms of required impulse and transfer times are computed, finding an ideal parking orbit for the mission. The launching phase is simulated in order to find the main parameters of a launcher vehicle capable of carrying the entire satellite system to the parking orbit. The sustainability aspects of the mission are analyzed. This includes an estimation of the cost, both for each subsystem and the launcher vehicle, yielding an estimated mission cost of less than USD 100M. The environmental impact of a mission of this kind is discussed, comparing the carbon dioxide emissions per rocket launch with a long-distance aeroplane flight. Furthermore, a short reflection on the social impact and importance of launching satellites is given. The paper concludes that the mission is not feasible at this moment in time due to the low technology readiness level of the propulsion subsystem.**

***Index Terms*—Space Mission, Debris Removal, Tethered-Net, SL-8 R/B, Satellite, LEO, Deorbit, Gravity Turn.**

NOMENCLATURE AND ACRONYMS

Ω	Right ascension of ascending node
ν	Mean anomaly
a	Semi-major axis
i	Inclination
e	Eccentricity
n	Mean motion
ω	Argument of the perigee
$\Delta\theta$	Relative angle of deployment
μ	Earth's standard gravitational parameter
M	Mach number
γ	Flight path angle
B^*	Ballistic coefficient of decay bodies
C_D	Drag coefficient
ρ	Air density

ADCS	Attitude Determination and Control System
ADR	Active Debris Removal
RAAN	Right Ascension of the Ascending Node
TRL	Technology Readiness Level

I. INTRODUCTION

THERE are currently over twelve thousand tracked debris objects in Low Earth Orbit (LEO). This approximately doubles the amount of debris since the turn of the current millennia [1]. Rising concerns of a potential chain reaction of colliding debris (due to the debris' high density in Low Earth Orbit), result in an escalating problem called the Kessler Syndrome [2]. This could potentially result in LEO being completely inaccessible in the near future, bringing the topic of Active Debris Removal (ADR) missions into the limelight. This paper covers a study of the feasibility of a one-year ADR mission to bring down multiple high-priority debris objects from LEO.

A. Mission Concept

The aim of the mission is to design a satellite system to descend 8 spent rocket stages from their current orbits to a lower altitude in less than 1 year. The final orbits must ensure a remaining orbital lifetime of no more than 25 years, typically lower or equal to the decay orbit of altitude $h_{decay} = 300$ km [3].

To meet the mission requirements, a novel design of a satellite system is proposed to optimize mission time and feasibility. This system is comprised of 8 CubeSat-originated spacecraft, each deorbiting one independent debris. They are all embedded in an external satellite bus to be launched to a parking orbit relatively close to the debris. Once the bus reaches the parking orbit, it will start deploying each spacecraft to the corresponding debris orbit when the desired relative positions between the bus and each debris are achieved. The deployed spacecraft will begin its mission in parallel and remove its target debris.

Each spacecraft requires an independent propulsion system. The propulsion strategy is low-thrust, using plasma-based thrusters with Xenon propellant. The debris is caught and taken down to a lower altitude, where drag forces will deorbit them. Each spacecraft will burn alongside its target debris during this period of time. Once the bus has deployed every spacecraft, it is deorbited from the parking orbit using its standalone propulsion.

B. Scope and Limitations

From a technical point of view, this paper includes: (1) a study of the existing ADR technology; (2) a selection of the space debris to remove; (3) a preliminary design of the spacecraft's major subsystems including an estimation of their power and mass; (4) a preliminary design and simulation of the ascent trajectory of an ideal launcher to meet the mission needs; (5) a study for the in-orbit manoeuvring including necessary impulse, propellant, mission and decay times.

Concerning sustainability and cost, this paper includes: (1) a preliminary analysis of the CO_2 emissions and cost of different launchers, with a discussion of their re-usability; (2) an estimation of cost for the spacecraft subsystems; (3) an approximation of the labour costs involved in the mission; (4) a comparison between the CO_2 emissions of aviation and space industries; (5) a general reflection on the importance of satellites in the space industry.

C. Requirements

The mission requirements are as follows:

(i) The chosen debris must be 8 spent rockets stages.
(ii) The debris must be taken down in less than one year.
(iii) The decay orbit must ensure that the debris will have a maximum orbital lifetime of fewer than 25 years.

The spacecraft requirements are:

(i) The 8 spacecrafts must fit into a parking orbit bus.
(ii) Each spacecraft must be able to communicate to Earth, sending its position with high accuracy and frequency.
(iii) The power subsystem must consist of enough battery capacity and solar power generation to sustain the rest of the subsystems.
(iv) The attitude and control subsystem must have the ability to re-orientate the spacecraft during the debris capture manoeuvres.
(v) The propulsion strategy has to be low-thrust, and each thruster must fit into each spacecraft frame.
(vi) The structure of the spacecraft must be capable of carrying the rest of the subsystems and withstanding the thruster loads.

The bus requirements are:

(i) The bus must fit into the launcher fairing in terms of mass and volume.
(ii) It must stay in the parking orbit until all the spacecraft are deployed, sending data about its position to the ground station.
(iii) Once all the spacecraft are deployed, the bus thrusts itself to a lower orbit where it decays in less than 25 years.

D. Active Debris Removal (ADR) literature survey

A deep analysis of existing technologies and similar missions is carried out. The following two missions are taken as inspiration sources for the present project:

(1) ClearSpace-1 (European Space Agency [4]): Mission aiming to remove a Vespa upper stage (112 kg) from orbit in 2026 with four robotic arms.
(2) RemoveDEBRIS (Surrey Space Center [5]): Mission launched in 2018, aiming to perform a series of experiments in-orbit on how to capture space debris with a harpoon, net, and a drag sail.

Regarding the different debris capture and deorbit methods:

(a) Harpoon: Tested by the RemoveDEBRIS mission. Medium Technology Readiness Level (TRL).
(b) Tethered-Net: Several net capture simulations and experiments have been carried out. Relatively high TRL.
(c) Robotic Arms: Tested in space environment, although not for debris removal missions. The European Robotic Arm of the ISS is an example. Relatively high TRL.
(d) Ion Beam Shepherd: An ion beam pointing at the debris, transmitting a deflecting impulse which effect is to eventually produce a large enough shift on the debris. Low TRL.
(e) Drag Sail: Additional area increasing the drag of the debris. Relatively high TRL.

Table I is included for the sake of comparing the specifications of different thrusters to allow the selection process on propulsion systems in Section II-A.

TABLE I: Spacecraft Thrusters State of the Art [6, 7].

Thruster	T [mN]	I_{sp} [sec]	Power [W]	Dry Mass [kg]
CubeSat MEMS	<4	110	<2.5	0.25
3D Printed	40	35	1.5	0.29
AMAC	425	220	20	1.20
PUC	5.4	72	15	0.45
CHIPS	30	82	30	0.50
CAT	4	800	55	1.00
BIT-3	1.15	2100	45	1.50
IFM Nano	0.4	3000	40	1.08
S-iEPS	0.074	1000	1.5	0.02

For the power subsystem, Table II is included to compare different batteries.

TABLE II: Battery Product State of the Art [1] [8].

Product	VED [Wh/dm^3]	SE [Wh/kg]	MDR [A]
NPD-002271	271.0	153.5	15.0
Nanopower BPX	228.7	150.0	2.5
Nanopower BP4	211.9	149.2	2.5
Optimus-40	169.5	119.0	2.6
28V Modular Batt.	151.1	109.8	20.0
VES16 4S1P	109.2	91.0	9.0
VLB-X	102.0	74.6	20.0

Regarding the solar panels, Table III includes a comparison of different solar cells.

TABLE III: Solar Cells State of the Art [8].

Company	Cell Name	BOL Efficiency	Pmp [W/m^2]
AZUR Space	4G32-Adv	31.5	431.0
SolAero	XTE-SF	31.9	433.4
SpectroLab	XTE-LF	31.3	427.9
Emcore	ZTJ	29.5	397.0

[1]Table II Nomenclature:
VED: stands for Volumetric Energy Density.
SE: stands for Specific Energy.
MDR: stands for Maximum Discharge Rate.

E. Motivation for selected ADR technology

After the initial ADR survey is conducted, the choice of ADR technology is between the harpoon system and the capture net system, as the robotic arm is deemed to be too complicated, and the ion beam shepherd in a too early stage of development. The drag sail has mostly been explored in combination with harpoon systems but could also potentially be used in combination with a capture net system. The RemoveDEBRIS [5] mission further displayed the robustness and relative simplicity of a capture net system, these findings combined with the relatively high TRL of a capture net system made this the chosen ADR technology of this study.

F. General Assumptions and Simplifications

In this paper, the following general assumptions and simplifications have been made:

(i) The debris is in the desired position at the desired time.
(ii) The thermal subsystem is not studied.
(iii) The low thrust propulsion strategy generates spiral transfer orbits.
(iv) The design of the subsystem's mechanics, electric circuit, and electronics is neglected.
(v) No taxes nor legal considerations are discussed.
(vi) Political and geographical considerations are not taken into account.

II. Methods

The methodology used in this study is explained in the present section. The main focus points are the dynamics of the launcher, simulations of the earth satellite operations, design of the spacecraft, debris selection, and cost and environmental impact analysis. The reader is referred to Section II-G for all the assumptions considered in the calculations

A. Spacecraft Subsystems Design

The main function of the spacecraft is to capture and deorbit space debris while also keeping the financial costs and environmental impact as low as possible. To fulfil these requirements, the mass and power consumption of the spacecraft has to be low. To estimate the mass, power consumption, and price of each spacecraft, the spacecraft is defined and analyzed in terms of a reduced number of subsystems.

(a) *Attitude Determination and Control System (ADCS):* The ADCS is used for determining the orientation of the spacecraft with the help of the geomagnetic field of the earth. It also stabilizes and changes the angular momentum of the spacecraft if needed.

(b) *Onboard Computer:* The main function of the computer is to execute commands transmitted from the ground station via the communication subsystem.

(c) *Communications:* A communications subsystem is needed to receive commands from the ground station as well as to transmit information back to the ground station.

(d) *Propulsion:* The selection of propulsion is based on the calculated thrust requirements and the state-of-the-art research summarised in Table I.

(e) *Structure:* A structure is needed to hold the various subsystems in place, for robustness a commercially available spacecraft frame will be selected. Despite the designed spacecraft not being classified as a "CubeSat" due to its significantly higher mass, CubeSat structure frames are looked into as the spacecraft has comparable geometries with CubeSats.

(f) *Capture Net:* The capture net, needed for the capturing manoeuvre of the mission, needs to be lightweight, flexible, and have sufficient tensile strength for the mission parameters. Additionally, it needs to be large enough to be able to wrap around the chosen debris.

(g) *Power Subsystem:* The batteries are scaled for the total power consumption of the spacecrafts, taking into account that the spacecrafts will spend roughly half of the time of each orbit in the earth's shadow. The state-of-the-art data obtained from NASA, as displayed in Table II will be used for the battery cell selection.

(h) *Solar Panels:* To recharge the batteries, solar panels are used. To select the solar panels, Table III is used to compare and select a suitable solar cell model. The table is an abbreviated version of a more extensive table by NASA [8] with the most efficient models prioritized as the mission will be power-intensive for its size. For the solar panel scaling the combined power consumption of all the subsystems will be considered as well as the time the spacecraft spends in sunlight, roughly half of the orbital period.

B. Bus Subsystems Design

The bus is a transportation means for the 8 spacecraft, enabling them to be launched together in one launch thus decreasing the costs and environmental impact. It is a larger spacecraft with similar subsystems as the spacecraft (with exception of a capture net). It will have ADCS, propulsion (for its deorbit manoeuvres), power storage, solar panels, a communications subsystem, and an onboard computer.

C. Selection of Space Debris

The choice of debris is determined based on the threat it poses to existing and future space missions. Considering available debris parameters (e.g. dimension, weight), several existing debris selection tables with a range of ranked debris in top importance are reviewed [9, 10]. In particular, eight Russian SL-8 R/B rocket stages, each weighing approximately 1.5 metric tonnes, are chosen to be removed with justified urgency [11]. These rocket stages are all left in orbit with similar altitudes and almost identical inclinations. Given the similar orbital parameters for the stages, the ΔV requirements of each spacecraft can possibly be reduced to reach them after

being deployed by the bus. They are therefore ideal as debris removal targets.

Orbital parameters for each stage, including inclination i, Right Ascension of the Ascending Node (RAAN) Ω, eccentricity e, argument of perigee ω, semi-major axis a, mean anomaly ν and mean motion n, are extracted from the Two Line Element [12]. Details of each selected debris with orbital parameters can be found in Table IV.

D. Rocket Performance and Dynamics

In order to launch the spacecraft into the parking orbit, the main propulsion parameters of an ideal rocket launch vehicle are designed and compared to commercial launchers to select the best vehicle for the mission needs. The rocket dynamics are simulated during the ascending phase of the vehicle by considering a gravity turn manoeuvre. The differential set of equations describing this manoeuvre is included in Eq. (1-5). Note that Eq. (3) takes into account Earth's curvature.

$$\dot{V} = \frac{T}{m} - \frac{D}{m} - g\sin\gamma \tag{1}$$

$$\dot{\gamma} = -\frac{1}{V}\left(g - \frac{V^2}{R_E + H}\right)\cos\gamma \tag{2}$$

$$\dot{X}_0 = \frac{R_E}{R_E + H} V\cos\gamma \tag{3}$$

$$\dot{H} = V\sin\gamma \tag{4}$$

$$\dot{m} = \frac{T}{I_{sp} g_0} \tag{5}$$

The thrust (T) is considered constant for each phase. The gravity (g) varies with height (H) as $g = g_0 \frac{R_E^2}{(R_E+H)^2}$. The drag force ($D$) is defined as $D = \frac{1}{2}\rho V^2 S C_D$. It is observed that only two rocket stages are needed to achieve the desired parking orbit. For the second stage, a steering law is defined in Eq. (6) to ensure a final path angle of zero degrees.

$$\tan\gamma(t) = \tan\gamma_1 \left(1 - \frac{t - t_{b_1}}{t_{b_2} - t_{b_1}}\right) \tag{6}$$

Note that γ_1 and t_{b_1} are the flight path angle and burn time when the first stage separation occurs, and t_{b_2} is the burnout time of the second stage. For the drag force computation, the density variation in height is modelled using the US standard atmosphere [13]. The drag coefficient is modelled using the relations defined in Eq. (7-10) [14].

$$M \leq 0.6 \;\rightarrow\; C_D = 0.15 \tag{7}$$

$$0.6 < M \leq 1.1 \;\rightarrow\; C_D = -4.32M^3 + 11.016M^2 - 8.5536M + 2.24952 \tag{8}$$

$$1.1 < M \leq 1.3 \;\rightarrow\; C_D = -M^2 + 2.2M - 0.79 \tag{9}$$

$$1.3 < M \leq 5.0 \;\rightarrow\; C_D = 0.16769 + \frac{0.17636}{\sqrt{M^2 - 1}} \tag{10}$$

Regarding the launch site, it is selected taking into account the restrictions of the chosen launcher, the additional impulse due to the location's latitude, and the inclination of launch (as it is needed to avoid flying over inhabited land).

E. Earth Satellite Operations

This section presents the methodology related to in-orbit manoeuvring. Three different impulses are taken into account:

(i) ΔV for semi-major axis change as ΔV_a:

$$\Delta V_a = \left|\sqrt{\frac{\mu}{r_i}} - \sqrt{\frac{\mu}{r_f}}\right| \tag{11}$$

(ii) ΔV for inclination change as ΔV_i:

$$\Delta V_i = V\sqrt{2 - 2\cos\frac{\pi}{2}\Delta i} \tag{12}$$

(iii) ΔV for RAAN change as ΔV_Ω:

$$\Delta V_\Omega = \frac{\pi}{2}\sqrt{\frac{\mu}{a}}|\Delta\Omega|\sin(i) \tag{13}$$

Once all the impulses are computed, Eq. (14) can be employed to estimate the necessary propellant mass. Concerning only the tangential impulse, the estimated time for a spiral transfer t_{spiral} can be computed with Eq. (15), see Appendix A for the derivation.

$$m_p = m_0\left[1 - \mathrm{e}^{-\frac{\Delta V_{tot}}{g_0 I_{sp}}}\right] \tag{14}$$

$$t_{spiral} = \frac{m_0 I_{sp} g_0}{T}\left[1 - \mathrm{e}^{\frac{1}{m_0 I_{sp} g_0}\left(\left|\sqrt{\frac{\mu}{r_i}} - \sqrt{\frac{\mu}{r_f}}\right|\right)}\right] \tag{15}$$

Note that m_0 is the initial mass, V_{tot} is the total impulse, r_i and r_f are the initial and final radius, respectively. Out-of-plane thrust manoeuvres are applied to change the inclination and RAAN, entering the debris orbit. Other orbital parameters (such as ω) are not considered due to the circular orbits assumption. At this point, the mission is divided into the following steps:

(a) *Parking Orbit Insertion:* The satellite system is brought to orbit at LEO by the launch vehicle defined in Section III-C. With the debris altitudes at a range of 970-990 km, the initial parking orbit is set at 1000 km to allow inner orbit transfer within a short duration. Using Eq. (12, 13), the parking orbit inclination i_{park} and RAAN Ω_{park} are optimized through numerical iterations such that ΔV_i and ΔV_Ω are minimized. The resultant parking orbit parameters are shown in Table IV and visualized in Figure 3, which the satellite system will reach.

(b) *Spacecrafts Deployment & Transfer Maneuver:* The debris-capturing spacecrafts are deployed in suitable locations such that they can intercept their target immediately when arrived at the debris orbit. The relative angle of deployment $\Delta\theta$ is thus determined to parameterize the spacecraft deployment location with respect to the debris position. It is computed by multiplying the orbital velocity of the debris with the spiral transfer time of the first manoeuvre. Each spacecraft performs an in-plane first spiral transfer maneuver with impulse ΔV_{a_1} during time t_{a_1}. Inclination and RAAN changes are done once it reaches its target debris altitude using discontinuous out-of-plane thrust. Separated ΔV_{i_1} and ΔV_{Ω_1} are inserted within time $t_{(\Omega+i)_1}$.

TABLE IV: SL-8 R/B Debris Orbital Parameters.

NORAD	Mass [kg]	B^* [m^2/kg]	h [km]	a [km]	i [deg]	RAAN [deg]	e	ω [deg]	ν [deg]
10732	1435	0.0254	987	7358	82.9290	256.9145	0.0018	253.9425	279.6022
21090	1435	0.0254	983	7354	82.9196	239.5448	0.0021	36.6689	323.5939
7594	1435	0.0254	974	7345	82.9434	288.1425	0.0016	334.7938	134.7383
23180	1435	0.0254	977	7348	82.9424	293.8407	0.0028	206.7981	263.0482
13917	1435	0.0254	982	7353	82.9401	251.4856	0.0027	243.5039	178.4573
12092	1435	0.0254	981	7352	82.9387	247.4303	0.0031	95.4440	26.0692
9044	1435	0.0254	990	7355	82.9827	288.0330	0.0013	279.6390	193.8914
10138	1435	0.0254	981	7364	82.9371	255.9318	0.0022	52.1912	66.3548
Parking orbit	300	0.0221	1000	7371	82.9392	266.7959	0	-	-

(c) *Debris Capture Operation:* Each spacecraft triggers a spring-loaded net deployment mechanism, this will release the net in a conical arrangement forwards and wrapping around its target.

(d) *Deorbit Maneuver:* Upon successful debris capture, each spacecraft re-orientates its thrusters and begins the deorbit manoeuvre with the debris. The spacecraft brings the debris from its original orbit to altitude at h_{decay} (similar operation to the transfer manoeuvre), and the impulse involves only a tangential ΔV_{a_2} with transfer time t_{a_2}.

(e) *Debris Decay:* Each spacecraft with captured debris reaches h_{decay}. The decay time t_{decay} is found by including atmospheric drag from an existing high-altitude Earth density model [13]. Selecting the corrected atmospheric drag coefficient $C_D = 2.35$ [15] for satellite bodies (unlike the conventional value at $C_D = 2.2$), the ballistic coefficient B^* of decay bodies (spacecraft and debris) is calculated by $B^* = C_D \frac{A}{m}$. The effective area for drag of each debris is $A = 15.804$ m^2 [11], while the mass m is the combined mass of one spacecraft and debris. Hence, t_{decay} is computed iteratively to add the Δt_{decay} defined in Eq. (16). The altitudes H_{ini} and H are the initial and intermediate altitudes in kilometres respectively. H_{scale} is evaluated from the closest available altitude to H from the density model by interpolation. The density ρ_0 is the air density at H_{ini}.

$$\Delta t_{decay} = -\frac{H_{\text{scale}}}{B^* \rho_0 \sqrt{\mu R_E}} \left[\mathrm{e}^{H/H_{\text{scale}}} - \mathrm{e}^{H_{\text{ini}}/H_{\text{scale}}} \right] \qquad (16)$$

(f) *Bus Deorbit:* The bus is decommissioned and deorbited itself after completing all spacecraft deployments, using its IFM thruster to reach h_{decay}, from where it begins its decommission. The effective area of the bus for the ballistic coefficient is found to be 0.5639 m^2, including its solar panels and utilizing their deployable surface to increase drag. The calculations give the bus $\Delta V_{tot} = \Delta V_{a_2}$, $t_{tot} = t_{a_2}$ and t_{decay}, which are given in Table VIII.

(g) *Propellant Mass Estimation:* Eq. (14) is used to compute the needed propellant mass, which is the summation of: (1) the propellant mass to get from the parking orbit to the debris, using the spacecraft's dry mass as $m_0 = 30$ kg; and (2) the propellant needed to carry the debris to h_{decay}, using $1,465$ kg as initial mass.

F. Sustainability and Cost

The sustainability analysis is done by comparing the carbon footprint of different launchers. The topic of re-usability is discussed, as it decreases the production costs of the launching system. Moreover, the carbon emissions of the aviation and space industries are compared, yielding the results explained in Section III-E.

The cost analysis is carried out by estimating the costs of (a) the present study work time, (b) the launcher, (c) the spacecraft, and (d) labour and production. Regarding the cost of the present study, it is computed taking into account a study workload of 500 hours. In regard to the launch cost, it depends on the number of kilograms sent and the destination. The spacecraft costs are computed by estimating the cost of each subsystem and adding them up. The labour costs are analyzed with two main simplifications: (1) the project is done in Sweden and (2) all the workers are engineers earning the average salary. Production and development times are based on similar missions' state-of-the-art.

G. Calculation Assumptions

The following assumptions are taken into account within the calculations:

(i) The angle-of-attack of the launcher is considered to be zero in order to neglect the lifting forces.
(ii) Given the low range of eccentricities ($e \sim 0.001$) for all debris, their orbits are assumed circular with a radius equal to their semi-major axis.
(iii) The spacecraft will approach the debris orbit in a quasi-tangential manner.
(iv) The calculation for impulse on the argument of periapsis ΔV_ω is neglected.
(v) The effect of atmospheric drag is neglected for the deorbit manoeuvre but will be considered in the orbital decay.
(vi) The spin of the debris is not considered.
(vii) The waiting time for deploying spacecrafts is not considered.
(viii) The Oblateness effect is considered only for RAAN manoeuvres.

III. Results

This section presents the results obtained in the design phase. Regarding the design of the subsystems, a separate analysis is carried out for the spacecraft (Section III-A) and for the bus (Section III-B).

A. Spacecraft Subsystems Design

A summary of the spacecraft subsystems' estimation of mass, power, and price is given in Table V.

TABLE V: Spacecraft Subsystems Analysis.

Component	Mass [kg]	Power [W]	Price [USD]
ADCS	0.20	1.2	9,570
Onboard Computer	0.05	5.5	40
Communications	0.66	7	31,850
Propulsion	6.00	330	390.000 [2]
Propellant	83.56	-	75,200
Structure	4.90	-	18,720
Capture Net	1.24	10	100
Power Storage	4.26	-	50,000
Solar Panels	12.60	-	350,000
Total	113.46	353.7	925,480

(a) *ADCS*: The IMTQ magnetorquer is employed, as it can fit the design and function of the spacecraft. The IMTQ uses an inbuilt magnetometer XEN1210, which is a 3-axis magnetometer that employs the Hall effect to measure the magnetic field [16]. For the attitude control of the spacecraft, the IMTQ magnetorquer is used alongside reaction wheels.

(b) *Onboard Computer:* A Raspberry Pi model 4 [17] is used to handle the software and data from the rest of the subsystems with a quad-core processor of up to 1.5 GHz processing speed, which is more than enough for all the expected commands and data that the processor has to handle in operating time. The inclusion of HDMI cable input could help make the selection of the space camera a lot easier since controlling the spacecraft during the debris capture is manual. An off-the-shelf camera is used to monitor the mission and ensure the spacecraft reach their destinations.

(c) *Communications:* For the communications subsystem, a UHF transceiver is used onboard the spacecraft to send and receive a rate of data up to 19 kbps configurable, with a frequency range of 400-403 MHz or 430-440 MHz [18]. The choice of the transceiver comes with the consideration of its low mass of 95 g and low cost. The low power consumption of 1 W helps with the mass of the batteries and solar panels. For the antenna, a UHF Antenna 2U is used for transmissions of the data. It has a commercial UHF frequency range 400-403 MHz and VHF frequency range of 144-148 MHz. It radiates radio power in all directions equally. It also has a low mass of 210 grams and low power consumption of 2 W.

(d) *Propulsion:* The propulsion strategy is low-thrust aforementioned. From Table I, Six CubeSat Ambipolar Thrusters (CAT) yielding 24 mN of total thrust are chosen for the requirements of this project. This is a plasma thruster that was originally developed by the Plasmadynamics and Electric Propulsion Laboratory at the University of Michigan and is now being matured by Phase Four [7, 19]. The total power requirement for the propulsion subsystem is 330 W, including the six thrusters. Based on Enpulsion [20] and Busek [21] similar commercial thrusters, the price range of their thrusters is between USD 30,000 and USD 100,000. As the CAT thruster is still in development, there is still no commercial cost for it. For this reason, an average cost of USD 65,000 is taken from similar products as a first estimation of the cost of each CAT.

(e) *Structure:* A pre-built 12U-CubeSat (12 units) frame by the company EnduroSat [22] is chosen to host the mission subsystems. Six CubeSat units host the thrusters (one unit each), one unit host the capture net, three units host the batteries, and two units host the ADCS, the onboard computer, and the communications system. The solar panels are folded and added to the outside of the CubeSat frame. This Endurosat frame costs USD 9,440. It has a weight of 2.44 kg, and the dimensions are $100 \times 226 \times 366$ mm. It is made of aluminium alloy 6082 (AW-6082-DIN 3.2315). This material has a Young's Modulus of 71 GPa, a density of 2.71 g/cm^3, a Yield Strength of 260 MPa and a melting point of 660°C [23].

(f) *Capture Net:* The capture net is 20 m^2 in size and the holes are 0.04 m^2. Made out of multiple strings of stainless steel wire, the net construction requires 200 meters of 1 mm diameter AISI 304 stainless steel string [24]. The chosen string has a melting point of 1400°C, a Young's modulus of 200 GPa, a Yield Strength of 240 MPa, and a density of 7.8 g/cm^3 [25]. The total weight is 1.24 kg and each strand of wire is capable of withstanding forces above 250 N with a safety factor of $\eta = 2$, which is several orders of magnitude above the thruster capabilities.

(g) *Power Subsystem:* According to Table V, the total power consumption at peak power usage is approximately 360 W, the battery needs to have a minimum capacity of $360\ \text{W} \cdot \frac{53\ \text{min}}{60\ \text{min/h}} = 318$ Wh. The VLB-X in Table II has a Volumetric Energy Density of 101.96 Wh/dm^3 and a Specific Energy of 74.6 Wh/kg, this would make the battery take up a volume of 3.12 litres or just above three units of the CubeSat volume, and weigh around 4.26 kg. For a price estimation, batteries of similar capacity but with a higher energy density cost approximately USD 50,000 [26]. This price is overestimated to this value for the sake of simplicity.

(h) *Solar Panels:* As seen in Table V, the potential peek power demand of the spacecraft is approximately 360 W, and the solar panel array has to be able to produce twice as much (approximately 720 W) as it will spend half of the time in the earth's shadow. Selecting the AZUR Space 4G32-Adv (431 W/m^2) it can be concluded that the solar panel array needs a total (effective) area of $\frac{720\ \text{W}}{431\text{W/m}^2} \approx 1.67$ m^2. To get an estimate of both the price and mass of such a solar panel array, data from comparable models [27] is used.

[2] An estimate of six thrusters based on the average price of similar products.

B. Bus Subsystems Design

The bus, with an equivalent size of 198U, is composed of a monolithic structure containing the 8 deorbit spacecraft (size of each $3 \times 4 \times 2$U) and its own satellite subsystems with a structural frame, which combines to form the whole satellite system design. The frame is made of aluminium alloy with additional reinforcements to withstand the structural load when deployed from the launcher, taking up a dimension of $6 \times 8 \times 4$U plus an extended 6×1U for the bus subsystems and accounting for more than 90% of the bus mass.

The spacecraft are stacked into 2 layers with a 4-up-4-down configuration, and an embedded deployment mechanism will be triggered to deliver all of them separately into orbit. The bus subsystems occupy a 3×2U unit including the same subsystems of one spacecraft without the net module and replacing the CAT, where the solar panels and batteries are resized to meet the power requirements. One IFM Nano Thruster [28] (denoted as IFM thruster later) with lower power consumption and mass is chosen as the propulsion system as the propulsion requirements are lower for the bus. Regarding the battery capacity and the solar panels' size, they were computed with the same procedure as for the spacecraft, which yielded the results in Table VI.

TABLE VI: Bus Subsystems Analysis.

Component	Mass [kg]	Power [W]	Price [USD]
ADCS	0.196	1.2	9,570
Onboard Computer	0.046	5.5	40
Comms System	1.320	14.0	53,700
Propulsion	1.300	40.0	30,000 [3]
Structure	55.098	-	154,440 [4]
Power Storage	0.840	-	10,000
Solar Panels	1.200	-	34,000
Total	60	62	291,750

C. Launcher Dynamics and Performance

The ascent trajectory is simulated with the parameters specified in Table VII, yielding the results shown in Figures 1 and 2. Note that the thrust and specific impulse are considered constant, and therefore averaged between sea level and zero-gravity conditions. Discussion is expanded in Section IV-A.

TABLE VII: Rocket Stages breakdown.

Variable	Nomenclature	First Stage	Second Stage
Thrust	T [kN]	3,904	374
Specific Impulse	I_{sp} [sec]	283	348
Structural Mass	m_s [kg]	25,600	3,900
Propellant Mass	m_p [kg]	150,370	35,210
Payload Mass	m_* [kg]	40,078	968
Cross-Section	S [m^2]	10.75	10.75
Velocity Increment	ΔV [m/sec]	2,231	5,122
Burn Time	t_b [sec]	107	322
Burnout Height	H [km]	85	1000

[3] IFM Nano Thruster Specifications [28, 29].

[4] Assuming that the price of this structure remains proportional to the price of the spacecraft structure.

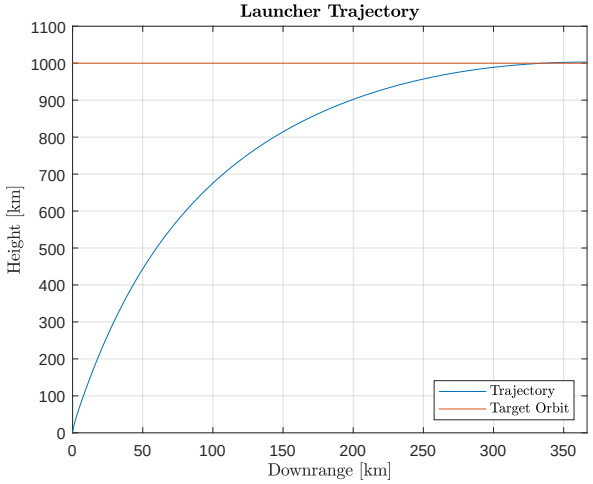

Fig. 1: Rocket Trajectory in Space.

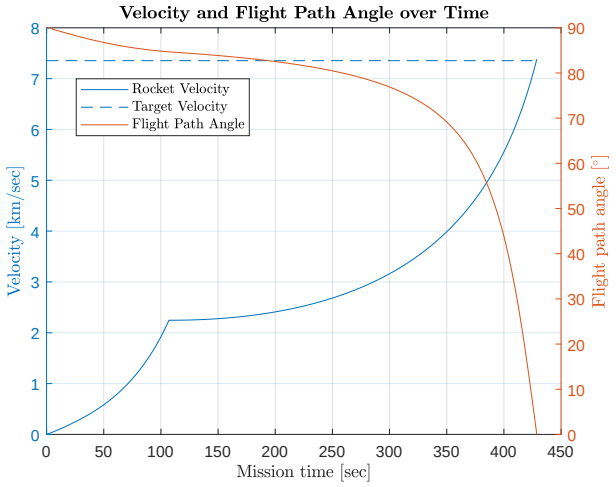

Fig. 2: Rocket Velocity and Flight Path Angle Over Time.

D. Earth Satellite Operations

Regarding the in-orbit operations, the results are shown in Table VIII. The debris and parking orbits are illustrated in Figure 3. For the sake of clarification, the first subscript of the variables in Table VIII is an orbital parameter, standing for the change of the corresponding variable during the manoeuvre associated with the particular orbital element. Furthermore, the second subscript ("1" or "2") stands for the transfer manoeuvres before or after capturing the debris, respectively. Discussion is carried out in Section IV-B.

E. Sustainability and Cost

The costs of each subsystem per spacecraft and bus are gathered in Table V and Table VI, respectively. This yields a total cost of USD 7,695,590 for the space segment. The launcher costs (specific price times the spacecraft mass) and CO_2 emissions are calculated for different launchers, yielding the results in Table IX.

TABLE VIII: Mission Specifications for Debris Removal and Bus Deorbit Results.

NORAD / Name	ΔV_{a_1} $[\frac{m}{s}]$	ΔV_{i_1} $[\frac{m}{s}]$	ΔV_{Ω_1} $[\frac{m}{s}]$	ΔV_{a_2} $[\frac{m}{s}]$	ΔV_{tot} $[\frac{m}{s}]$	t_{a_1} [min]	$t_{(\Omega+i)_1}$ [d]	t_{a_2} [d]	t_{tot} [d]	t_{decay}	$\Delta\theta$ [deg]
10732	6	2	1971	370	2349	260	100	261	361	18y 343d	86.0374
21090	8	4	5438	368	5818	340	100	259	359	18y 343d	224.3119
7594	13	0.8	4305	364	4681	527	100	256	356	18y 343d	187.3603
23180	11	0.6	5438	365	5815	460	100	258	358	18y 343d	70.6381
13917	9	0.2	3045	367	3422	374	100	259	359	18y 343d	283.2384
12092	9	0.1	3855	367	4232	387	100	259	359	18y 343d	305.0204
9044	8	9	4262	368	4647	325	100	260	360	18y 343d	197.4170
10138	4	0.4	2178	372	2555	155	100	263	363	18y 343d	265.6707
Bus	-	-	-	376	376	-	-	649	649	21y 112d	-

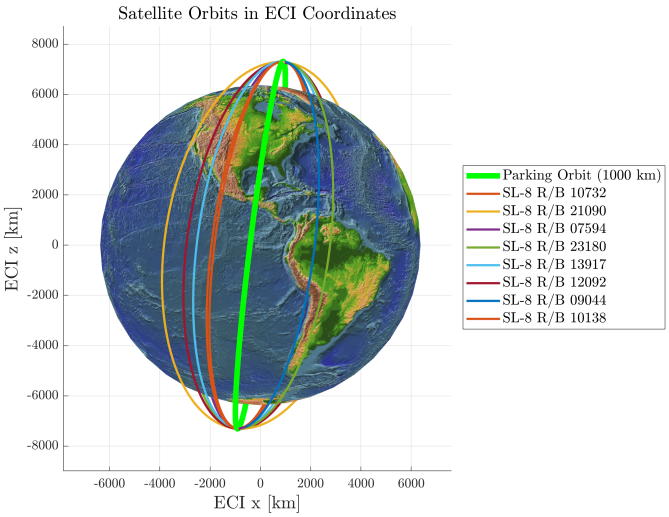

Fig. 3: Debris and Parking Orbits Visualization.

TABLE IX: Launcher Cost and Carbon Footprint for Different Launchers [30, 31].

Launcher	Launch Price [USD]	CO_2 Emissions (tonnes)
Falcon 9	2,612,520	425
Ariane 5G	12,675,560	189
Soyuz	7,353,760	243
ATLAS V	8,219,500	259

Regarding the costs of the present study, its workload is 500 hours divided among 4 engineers. An average salary of USD 24 per hour is considered, yielding USD 12,065. Regarding the production and testing process time, it is estimated to take around 5 years with a delay buffer of 2 years (from the state-of-the-art similar missions). The estimated workforce required given the scale of the project is about 100 engineers, which leads to lower expected costs, around USD 23,136,000 and upper costs of USD 32,390,400 considering delays.

As shown in Table IX, the total carbon emissions for Falcon 9 is 425 metric tonnes and a Boeing 737-400 produces 115 grams of CO_2 per passenger every kilometre. The required distance for a full Boeing 737-400 to reach 425 metric tonnes of carbon emissions is 19,658 km, which is the equivalent of a round-trip from Hong Kong to London. Given that the number of aviation flights is way higher than the number of space launches, spaceflight's impact on the environment is really low compared to the impact of aviation.

IV. Discussion

The present section discusses the obtained results, making emphasis on the launcher, in-orbit manoeuvring, sustainability, cost and TRL.

A. Rocket Performance and Dynamics

Regarding the launcher, Figure 1 illustrates its trajectory in space, starting from sea level and ending in the parking orbit of 1000 km. The total downrange distance is about 365 km. Figure 2 shows the evolution of the flight path angle and velocity in time. As the rocket starts from a vertical position and transitions horizontally, the flight path angle goes from 90° to 0° over time. Regarding the velocity, there is a change in the curve at the first stage separation around $t = 107$ sec, as the sudden change in the mass of the launcher produces an abrupt change in acceleration. The final velocity of the launch vehicle is 7,353 m/sec, corresponding to the orbital velocity of the parking orbit.

These launcher specifications are comparable with a SpaceX Falcon 9 launcher. The structural mass of the designed rocket and Falcon 9 are identical. Furthermore, it can carry a payload mass of 22,800 kg, it is reusable and the price per lifted kilogram is reasonable. The specific impulses and cross-sections are identical. The thrust ratios between the designed rocket and a Falcon 9 (T/T_{F9}) are 50% and 40% for the first and second stages, respectively. Regarding the propellant mass ratios $(m_p/m_{p_{F9}})$, it is 38% for both stages. A Falcon 9 rocket can perform better than the designed rocket, thus it is capable of lifting the desired payload to the desired orbit without major inconvenience.

Falcon 9 comprises two stages. It has a total height of 70 m, a cross-sectional diameter of 3.7 m and an operating empty weight of 549,054 kg. It uses LOX / RP-1 as propellant. The launch site for this vehicle is Launch Complex 39A in Kennedy Space Center on Merritt Island in Florida, United States. It is at a latitude of 28.5735° north. Launching to the east will save extra fuel for the equatorial motion of Earth, this effect is in the order of 463 m/sec for the equatorial plane and 407 m/sec for the launch site in Florida. Therefore, there is a difference of 56 m/sec that is not taken advantage of for political and geographical reasons. The launch will be performed in the direction of the Atlantic ocean avoiding land. For more information, the reader is referred to reference [32].

B. Earth Satellite Operations

Regarding the in-orbit manoeuvring, it is worth noticing the small contribution in the total impulse of ΔV_{a_1} and ΔV_{i_1}, compared to ΔV_{Ω_1}, as RAAN change dominates the requirements on impulses (c.f. Table VIII). Drag is neglected in the transfer manoeuvres, but its actual effect would favour lowering the mission time. Complex debris capture mechanics due to the debris spin may incur an increase in the total impulse, while the omitted waiting time for reaching a correct $\Delta\theta$ (c.f. Section II-E) can highly prolong the actual mission. Regarding the mission time, the longest deorbit manoeuvre takes 363 days, with a decay time of almost 19 years. The bus is deorbited in 649 days, with a decay time of fewer than 22 years.

C. Sustainability and Cost

For the spacecraft cost, the most expensive parts are the solar panels and the propulsion system due to the need for subsystems with high capabilities for the long-range manoeuvres that the spacecraft have to conduct to reach their destinations. These two subsystems, alongside power storage, make up the majority of the spacecraft's weight, which means that they impact the launch costs. The cost analysis of labour is a rough estimation and not good enough considering taxes, insurance, and damages during work. The work time and manpower are based on similar missions.

From Table IX it is observed that the Ariane 5G is the most efficient launcher when considering launch carbon footprint, mainly because of its main cryogenic engine that uses hydrogen and liquid oxygen as propellant. Cost wise the Falcon 9 is the most efficient, but it has a greater launch carbon footprint compared to other launchers. This analysis does not take into account that Falcon 9 is reusable, which radically reduces the environmental impact of its production. For more information, the reader is referred to [33].

The space industry is a vital factor in a wide range of industries, as it helps to reduce the carbon footprint in an indirect way by offering companies and organizations the option to do remote meetings and data networking, reducing emissions of transportation. It also offers the ability to share information using the internet instead of the old paper-bound methods at remote or underdeveloped locations. Furthermore, satellites offer an understanding of both the climate and weather which was not possible before the era of spaceflight. It can not be ignored that the world is satellite-dependent, despite the inherited environmental (and atmospheric) problems of launching satellites, and the potential for debris after a failed deorbit or a collision with existing debris.

D. Technology Readiness Level

TRL measures the maturity of a technological product or design during its acquisition phase, which can provide a direct measurement of the feasibility of the ADR mission by comparing TRL on each component within the entire mission. The TRL of the launcher, satellite subsystems (for both spacecraft and bus) and debris-capturing method are analyzed.

The selected Falcon 9 launcher has delivered multiple missions with TRL 9. The chosen net capture system has a high TRL at 8-9 as well, as it has been tested and flown in space. For the satellite subsystems, the onboard computer, ADCS, Communication system, solar panels, batteries and structural frames have been fully tested and flown in space, giving them the status at TRL 8-9. For the Propulsion, while the IFM thruster installed in the bus is commercially available for missions with TRL 8, the main problem lies within the CAT in the spacecraft, which is neither fully tested nor commercialized, giving a lower TRL of 4. Therefore, the mission is not yet feasible until the TRL of CAT increases to higher than TRL 7 while all other satellite components stay constant.

V. Conclusion

A preliminary analysis of an ADR mission is carried out according to the requirements. From the technical point of view, the different phases of the mission are empirically designed, with emphasis on the spacecraft subsystems, in-orbit operations and launcher vehicles. The cost and environmental impact are both analysed, providing a sustainability perspective on different mission phases and their role. The cost of the mission is estimated to be around USD 50 million, which could be doubled due to the simplifications made during the calculations, yielding an estimated cost of USD 100 million. The components used in the spacecraft have a relatively high TRL, except for the CAT propulsion which only has a prototype built and lab-tested. The mission is thus not feasible until the propulsion system is fully tested and commercially available. Nevertheless, all the mission requirements are met during the design phase, concluding it to be satisfactory.

For future work, further reductions in costs can be done through more detailed planning and analysis of the mission, as the current cost has a safety margin of USD 50 million and a long risk time delay. The power subsystem can be optimized and further analysed which can help reduce the capability and weight of this subsystem in all the spacecraft, ultimately reducing the costs and mass of the launch and spacecraft. The net capture mechanism can be further investigated with an emphasis on forces involved in the capture manoeuvre and mitigation of the induced angular momentum by it.

VI. Division of work

This project was divided into four main sections: the Launcher, Orbital Mission, Spacecraft Design and Sustainability Analysis. Each project member is responsible for one section with the division of work as follows.

- *Launcher*: Francesc Hernández Garcia.
- *Orbital Mission*: Ngai Nam Chan.
- *Spacecraft Design*: Simon Lilja.
- *Sustainability Analysis*: Marcus Mhanna.

Concerning overlapping contents such as the cost analysis and environmental impacts and spacecraft design caused by different components within the debris removal mission, members coordinate with each other to align with the project deliveries and ensure coherence between sections.

REFERENCES

[1] Boley A.C. and Byers M. "Satellite mega-constellations create risks in Low Earth Orbit, the atmosphere and on Earth." In: *Nature* (2021). DOI: https://doi.org/10.1038/s41598-021-89909-7.

[2] Mike Wall. *Kessler Syndrome and the space debris problem*. Nov. 2021. URL: https://www.space.com/kessler-syndrome-space-debris.

[3] *ESA - Space debris mitigation: the case for a code of conduct*. https://www.esa.int/Enabling_Support/Operations / Space_debris_mitigation_the_case_for_a_code_of_conduct. (Accessed on 10/01/2022).

[4] *ESA - ClearSpace-1*. https://www.esa.int/Space_Safety/ClearSpace-1. (Accessed on 10/15/2022).

[5] *RemoveDEBRIS mission — University of Surrey*. https://www.surrey.ac.uk/surrey-space-centre/missions/removedebris. (Accessed on 10/15/2022).

[6] Edgar A. Bering et al. "MarsCAT: Mars array of ionospheric research satellites using the cubesat ambipolar thruster". In: vol. 0. 2016. DOI: 10.2514/6.2016-1466.

[7] Khary I. Parker. "State-of-the-Art for Small Satellite Propulsion Systems". In: *Biennial Aerospace Systems Conference of the National Society of Black Engineers* (2016).

[8] *Power State of the Art — NASA Report*. https://www.nasa.gov/smallsat-institute/sst-soa/power. (Accessed on 10/03/2022).

[9] Satomi Kawamoto et al. "Considerations on the lists of the top 50 debris removal targets". In: *Journal of Space Safety Engineering* 9 (3 Sept. 2022), pp. 455–463. ISSN: 2468-8967. DOI: 10.1016/J.JSSE.2022.05.006.

[10] Darren McKnight et al. "Identifying the 50 statistically-most-concerning derelict objects in LEO". In: *Acta Astronautica* 181 (2021). ISSN: 00945765. DOI: 10.1016/j.actaastro.2021.01.021.

[11] Susanne Peters, Roger Förstner, and Hauke Fiedler. "Mission Architecture For Active Space Debris Removal Using The Example of SL-8 Rocket Bodies". In: Oct. 2014. ISBN: 978-3-319-15981-2. DOI: 10.1007/978-3-319-15982-9.

[12] *Live real time satellite tracking and predictions*. https://www.n2yo.com/. (Accessed on 10/04/2022).

[13] US Standard Atmosphere. *US standard atmosphere*. National Oceanic and Atmospheric Administration, 1976.

[14] G.P. Sutton and O. Biblarz. *Rocket Propulsion Elements*. A Wiley Interscience publication. Wiley, 2001. ISBN: 9780471326427.

[15] Mildred M. Moe, Steven D. Wallace, and Kenneth Moe. "Refinements in determining satellite drag coefficients - Method for resolving density discrepancies". In: *Journal of Guidance, Control, and Dynamics* 16 (3 1993), pp. 441–445. ISSN: 07315090. DOI: 10.2514/3.21029.

[16] ISIS Space. *iMTQ User Manual*. English. ISIS Space. July 22, 2015. 62 pp.

[17] Hirak Ghael. "A Review Paper on Raspberry Pi and its Applications". In: (Jan. 2020). DOI: 10.35629/5252-0212225227.

[18] EnduroSat. *UHF Transceiver II CubeSat Communication — CubeSat by EnduroSat*. https://www.endurosat.com/cubesat-store/cubesat-communication-modules/uhf-transceiver-ii/\#request-step-modal. (Accessed on 10/04/2022). 2022.

[19] J. P. Sheehan et al. "Initial operation of the CubeSat Ambipolar Thruster". In: *2015 IEEE International Conference on Plasma Sciences (ICOPS)*. 2015, pp. 1–1. DOI: 10.1109/PLASMA.2015.7179981.

[20] *Enpulsion - Order*. https://www.enpulsion.com/order/. (Accessed on 10/04/2022).

[21] *Busek - Hall Thrusters*. https://www.busek.com/hall-thrusters. (Accessed on 10/04/2022).

[22] EnduroSat. *12U CUBESAT STRUCTURE*. 2022. URL: https://endurosat.com/cubesat-store/cubesat-structures/12u-cubesat-structure/.

[23] *Properties of the Aluminum Alloy 6082*. https://www.makeitfrom.com/material-properties/6082-AlSi1MgMn-3.2315-H30-A96082-Aluminum/. (Accessed on 10/04/2022).

[24] AGST Draht & Biegetechnik GmbH. *V2A stainless — 0,6 mm to 1,2 mm*. 2022. URL: https://en.wire-shop.com/product-page/060mm-090mm-4301-aisi304.

[25] Matmatch GmbH. *AISI 304 Annealed - Austenitic Stainless Steel*. 2022. URL: https://matmatch.com/materials/mitf429-aisi-304-annealed.

[26] CubeSatShop. *EXA TITAN-1 350Whr High Energy Density Battery Matrix*. 2022. URL: https://www.cubesatshop.com/product/titan-1-high-energy-density-battery-matrix/.

[27] CubeSatShop. *Single CubeSat Solar Panels*. 2022. URL: https://www.cubesatshop.com/product/single-cubesat-solar-panels/.

[28] *ENP2019-086.B - IFM Nano Thruster COTS+ Product Overview*. https://www.enpulsion.com/wp-content/uploads/ENP2019-086.B-IFM-Nano-Thruster-COTS-Product-Overview-1.pdf. (Accessed on 10/01/2022).

[29] *IFM Micro Thruster*. https://ec.europa.eu/research/participants/documents/downloadPublic?documentIds=080166e5bd847266 & appId = PPGMS. (Accessed on 10/01/2022).

[30] Harry Jones. "The recent large reduction in space launch cost". In: 48th International Conference on Environmental Systems. 2018.

[31] Florian Kordina. *What is the environmental impact rockets have on our air?* 2020. URL: https://everydayastronaut.com/rocket-pollution/.

[32] *SpaceX - Falcon 9*. https://www.spacex.com/vehicles/falcon-9/. (Accessed on 10/03/2022).

[33] J.A. Dallas et al. "The environmental impact of emissions from space launches: A comprehensive review". In: *Journal of Cleaner Production* 255 (2020). DOI: https://doi.org/10.1016/j.jclepro.2020.120209.

APPENDIX A
DERIVATION OF EQUATION 15.

The well-known rocket equation is given by:

$$\Delta V = I_{sp} g_0 \ln\left(\frac{m_0}{m_0 - m_p}\right), \tag{17}$$

where m_p is the propellant mass used during the impulse. For low-thrust transfer, the initial-to-final mass ratio $\frac{m_0}{m_0 - m_p}$ can be expressed in terms of thrust and total transfer time by:

$$\begin{aligned}
\frac{m_0}{m_0 - m_p} &= \frac{m_0}{m_0 - \dot{m}_e\, t_{spiral}} \\
\frac{m_0}{m_0 - m_p} &= \left(1 - \frac{\dot{m}_e\, t_{spiral}}{m_0}\right)^{-1} \\
\frac{m_0}{m_0 - m_p} &= \left(1 - \frac{T}{m_0 I_{sp} g_0} \cdot t_{spiral}\right)^{-1}
\end{aligned} \tag{18}$$

Assuming only tangential impulse, the derivation for the estimated spiral transfer time can be done by Eq. (11,17,18) as follows:

$$\begin{aligned}
\Delta V_a &= I_{sp} g_0 \ln\left(1 - \frac{T}{m_0 I_{sp} g_0} \cdot t_{spiral}\right) \\
\left|\sqrt{\frac{\mu}{a_0}} - \sqrt{\frac{\mu}{a_1}}\right| &= I_{sp} g_0 \ln\left(1 - \frac{T}{m_0 I_{sp} g_0} \cdot t_{spiral}\right)
\end{aligned}$$

$$t_{spiral} = \frac{m_0 I_{sp} g_0}{T}\left[1 - \mathrm{e}^{\frac{1}{m_0 I_{sp} g_0}\left(\left|\sqrt{\frac{\mu}{a_0}} - \sqrt{\frac{\mu}{a_1}}\right|\right)}\right],$$

which arrives at Eq. (15).